J. Nano- Electron. Phys.
3 (2011) No1, P. 243-253

PACS numbers: 85.85. – j, 62.40. – i

REVIEW OF MEMS TEST STRUCTURES FOR MECHANICAL PARAMETER EXTRACTION

A. Sharma[1], ***M. Kaur***[1], ***D. Bansal***[1], ***D. Kumar***[2], ***K. Rangra***[1]

[1] Central Electronics Engineering Research Institute/Council of Scientific & Industrial Research (CEERI/CSIR), Sensors and Nanotechnology Group, Pilani 333031, Rajasthan, India
E-mails: kjrangra@gmail.com, akshdeepsharma@gmail.com

[2] Department of Electronics Sciences,
Kurukshetra University, Kurukshetra 136119, Haryana, India
E-mail: dineshelectronics@gmail.com

This paper reviews the recent progress in MEMS test structures for mechanical parameter extraction. MEMS test structures reviewed include cantilevers, fixed-fixed beams, bent-beam, guckel rings, pointers, circular diaphragm, and lancet structures. Important mechanical and process parameters are highlighted, as they have significant contributions to the performance of MEMS devices. The challenges and statues of the test structures are outlined and discussed.

Keywords: *MEMS TEST STRUCTURES, RESIDUAL STRESS, STRESS GRADIENT, YOUNG'S MODULUS, POISSON RATIO, PULL- IN VOLTAGE.*

(Received 04 February 2011, in final form 03 May 2011)

1. INTRODUCTION

The mechanical properties of the material used in microelectromechanical system (MEMS) fabrication are of fundamental importance. This knowledge is needed for the design of devices, and measurement of properties is needed to check the consistency of material during fabrication [1]. Since the material properties are sensitive to small changes in process, it is desirable to be able to determine wafer to wafer variation [2]. The development of technology characterization capability is essential to process monitoring which ensures the technology processing is consistent from run to run. Also, in-situ monitoring of some parameters may be quite beneficial to design development and qualification [3]. In the first section various test techniques to characterize mechanical properties are reviewed and in the second section of the review include in-situ structures used for residual stress measurement.

2. THE TEST TECHNIQUES

Techniques for the characterization of the mechanical properties of MEMS materials include the tension test, bend tests (microbeam bending, bulge test, M-test, and wafer curvature tests). Each of these techniques is considered in detail with reference to: (i) the mechanical properties that can be measured; (ii) the types of structures (i.e., integrated or nonintegrated, thin or thick, free-standing or constrained) that can be characterized and the ease of specimen fabrication; (iii) the ease of instrumentation and

fixturing (including the availability of commercial instruments); and (iv) the ease of data reduction and parameter extraction (especially, the need for intensive computation and the sensitivity of the technique to metrology).

2.1 The Tension Test

The microscale tension test is a natural extension of its macroscale counterpart, and can characterize the Young modulus, yield strength, and fracture strength of nonintegrated, free-standing, thin and thick structures. A uniaxial, tensile load is applied to a specimen with a gage section of uniform geometry, and the extension of the gage is recorded as a function of the applied load. Given the dimensions of the beam, it is straightforward to obtain a stress-strain graph, and to extract Young modulus (E), yield strength (σ_y), andfracture strength (σ_F).

The principal difficulty associated with this technique is the handling and mounting of the test structures. In the case of brittle materials, fracture induced by gripping presents an additional problem. One solution adopted by many researchers is to fabricate the test structure in a protective frame, and to sever the frame mechanically after mounting [4], and pull tests inside a scanning electron microscope [5, 6] have also been demonstrated. Materials that have been characterized using tensile test include single-crystal silicon, polysilicon [7], aluminum, nickel, copper and silver [8, 9].

2.2 Microbeam Bend Test

Microbeam bending has been extensively used to characterize the Young modulus, yield strength, and fracture strength of non-integrated, free-standing, thin and thick structures.

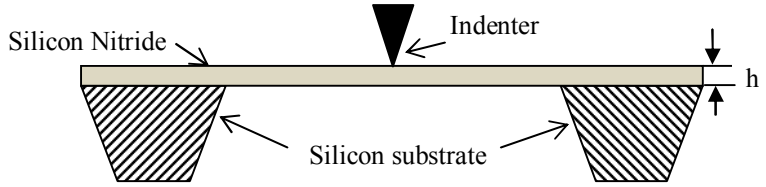

Fig. 1 *– Schematic illustration of the microbridge bend test*

A concentrated bending load (P) is applied to a beam (either cantilevered or fixed at both ends as shown in Fig. 1) and the displacement (δ) is recorded as a function of the load. In the early studies, values for the elastic constant and strengths were obtained by using simple analytical formulae [10-12]. For a cantilever beam of length L, width b, and thickness h, the Young modulus and fracture strength is given by the expressions

$$E = \frac{4(1-\nu^2)L^3}{bh^3}\frac{P}{\delta} \tag{1}$$

$$\sigma_F = \frac{6LP_F}{bh^2} \tag{2}$$

where P_F is the load at fracture. The preceding equations assume perfectly rigid support behavior and are valid in the small deformation regime. Both

these assumptions are violated in many microscale tests, and numerical analyses using finite-element techniques are necessary to interpret the data [13].Materials that have been characterized using bending tests include single-crystal silicon, silicon oxide, gold [14] and silicon nitride.

2.3 The Bulge Test

The bulge test is one of the earliest techniques used to measure the Young modulus and residual stress of nonintegrated, free-standing thin film structures. The specimen is a membrane (circular, square, or rectangular in shape) bonded along its periphery to a supporting frame. Microfabrication techniques are particularly well suited for the creation of such test structures with reproducible and well-defined boundary conditions. The membrane is pressurized from one side, and the deflection at the center (δ) is recorded as a function of the applied pressure (p), as illustrated in Fig. 2.

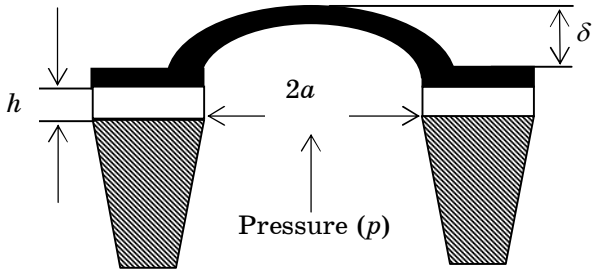

Fig. 2 *– Schematic Illustration of A Bulge Test*

For rectangular membranes (with thickness h and edge length $2a$), the pressure-displacement relationship is given as

$$p = C_1 \frac{h\sigma_R}{a^2}\delta + C_2(\nu)\frac{hE}{a^4}\delta^3 \tag{3}$$

The constant C_1 and $C_2(\nu)$ are determined using finite element analyses, and have values of 3.45 and 2.48 for $\nu = 0.25$, respectively [15]. In addition, the value of the Poisson ratio can be estimated by sequentially testing membranes with square and rectangular geometries [16].Materials that have been characterized using the bulge test include polysilicon [17], silicon nitride, and polyimide.

2.4 The M-Test

The M-test is an electrostatic beam bending technique use to measure the Young modulus and residual stresses of integrated, free-standing, and thin structures. The M-test relies upon the detection of such a collapse. Osterberg and Senturia identified several requirements for an ideal test including: (i) two conductors, one flat, parallel, and movable with respect to the second, which is a fixed infinite ground plane; (ii) perfectly fixed boundary conditions for the movable conductor; (iii) well-defined prismatic cross-section of the movable conductor; and (iv) negligible stress gradients in the movable conductor. The stress and modulus parameters are defined as

$$S = \bar{\sigma} h g_0^3 (4), \quad B = \bar{E} h^2 g_0^3 (5), \quad K = \sqrt{\frac{12S}{B}} \tag{6}$$

The effective modulus $\bar{E}$ is equal to $E/(1 - \nu^2)$ and E for wide and narrow beams, respectively. The effective stress $\bar{\sigma}$ is zero for cantilevers and equal to $\sigma_R(1 - \nu)$ for fixed-fixed beams. It is clear from Eqs. (4)-(6) that accurate measurement of the gap size and beam thickness is critical for the success of this technique. Under ideal conditions, the M-test can determine values of the modulus to within 4 %, as demonstrated in the case of single-crystal silicon structures [18]. Unfortunately, most surface-micromachined structures violate some, or all, of the conditions of ideality. In particular, the fabrication of rigid supports represents a significant design challenge. Therefore, computation using finite-element or finite-difference techniques is required to extract the Young modulus. Jensen et al. [19] report on measurements of the Young modulus of polysilicon to within 5 % using such techniques.

2.5 Wafer Curvature Test

The wafer curvature test has emerged as a popular technique for the evaluation of residual stresses in non-integrated, constrained, thin and thick structures, particularly, continuous films deposited on thick substrates. For small deformations, and when the film thickness (h_f) is much smaller than the thickness of the substrate (h_s), the magnitude of the residual stress in the film is given by the Stoney formula as [20]:

$$\sigma_R = \frac{1}{6}\left[\frac{E_s}{1-\nu_s}\right]\frac{h_s}{h_f}\kappa = \frac{1}{6}\left[M_s\right]\frac{h_s}{h_f}\kappa\,, \tag{7}$$

where κ is the curvature of the film-substrate composite (which can be measured using surface profiler), M is the biaxial modulus, and the subscript s denotes the substrate. It is important to note that the stress can be evaluated without any knowledge of the mechanical properties of the film.

3. STRESS MEASUREMENT STRUCTURES

The greater understanding of stress with in deposited thin films needs for surface micromachining. The numbers of structures are available in literature for past decade to residual stress measurement. These are array of structures for measuring compressive or tensile stress. Excessive compressive or tensile stress results in buckling, cracking, splintering and sticking problems. In particular, the residual stress is very important in MEMS application. In cases where thin film is designed to be a moving part, the mechanical displacement of the film largely affected by stress [21]. In this section several type of stress measurement techniques are reviewed in detail. When the structures under stress are released by removing sacrificial layer, the stress is relieved by increasing or decreasing the structure dimension. The change in dimension is very small, making direct measurement difficult. It is therefore necessary to convert this change into large displacement. At the end of this section these types of residual stress measurement techniques are highlighted.

3.1 In situ Stress Measurement Techniques

The conventional stress measurement method is the wafer curvature to calculate the average stress using Stoney equation; nanoindentation [22] or X- Ray diffraction techniques [23].The most popular and simplest method is the micromachining technique as it does not require special equipment and can be done by in situ measure.The micromachining technique is the focus of this section. Essentially, the test structure under stress is released after removing the underline sacrificial layer. The structure will deform by increasing or decreasing the dimension of structure because of residual stress. The stress can thus be derived from this deformation.The test structures that measure this stress can be separated into two main families according to the primary measurement technique used to extract the residual stress value: in-plane (pointers and bent-beams) and out-of-plane(microrings and fixed-fixed beams).Several types of micromachining technique of stress measurement are described in detail as follows.

3.1.1 Buckling Technique

Stress in the thin film results in an extension or contraction of the released structure. This is basic principle of the stress measurement by buckling technique.The typical device normally used is a micro bridge (free standing, double clamped micromechanical beam shown in appendix), can only measure compressive stress. A micro bridge that is under compressive stress buckles after release. The stress can be expressed using critical buckled bridge dimensions as Eq. (8).

$$\sigma = \frac{E}{1-\nu}\frac{\pi^2 h^2}{3L^2} \tag{8}$$

where E is the elastic modulus, ν is Poisson's ratio and $E/(1-\nu)$ is the biaxial modulus, L is the length of the critical buckled bridge, and h is the thickness of the bridge. Therefore, by fabricating beams with a range of different lengths shown in appendix Fig. A, B and observing the critical length beyond which buckling occurs, the residual stress in the structure can be evaluated.

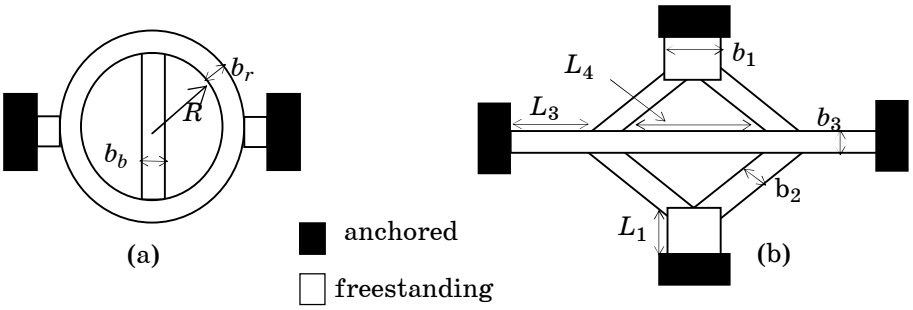

Fig. 3 *– Conversion structures for stress measurement Ring (a), Diamond (b)*

For tensile stress, the conversion structures shown in Fig. 3 are needed. The ring structure proposed by Guckel et al. [24] in Fig. 3 a can be used to measure tensile stress only. When the freestanding structure is released, the ring in Fig. 3 a deforms to an oval under tensile stress and the central beam

becomes compressive [25]. After removing the sacrificial layer in diamond structure Fig. 3 b, the diagonal beams convert the tensile stress into compressive stress in the middle beam and the compressive stress is increased in the outside beams, causing the middle beam to buckle with tensile stress and the outside beams to buckle when the stress is compressive stress [26].

3.1.2 Rotating Technique

The micromachined rotating structures as first presented by Goosen et al. [27] is shown in Fig. 4 a. The device consists of two test beams and a rotating pointer beam. One end of each test beam is anchored to the substrate and the other is connected to the pointer. When the test beams are released by etching away the sacrificial layer, they are elongated or contracted due to the residual stresses. The test beams are slightly separated at the connection to the pointer beam, thus create a rotating deflection of the pointer beam. The deflection is directly proportional to the residual stress in the thin film. Its direction corresponds to the type of stress, i.e. tensile or compressive stress. The residual stress can be calculated by following equation

$$\sigma = \frac{E}{1-\nu}\frac{O}{(L_A + L_B)(L_C + 0.5O)}\delta\,. \tag{9}$$

3.1.3 Pointers

Pointers are in-plane test structures that make use of geometric layout to amplify small displacements induced by residual stress. The amplified output of the pointer is measured on a scale attached to the substrate. The test beam lengths, L_A and L_B, are typically identical. Increasing the length of L_C or decreasing the separation distance O will enhance the amplification effect. Displacement readings at the pointer end are used to calculate the residual stress levels. This deflection of the pointer can be determined quite easily using an optical microscope or SEM.

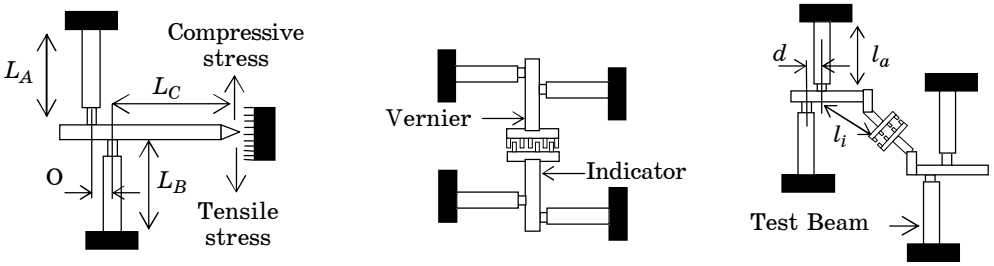

***Fig. 4** – The schematic of rotating techniques structures Pointer (a), double indicator (b), folded indicator (c)*

There are some improved test structures designed for using this technique in the literatures. As examples, two improved typical structures are described as follows. One of the improved test structures is the *double indicator structure* [26]. It can increase the sensitivity of the measurement by using two symmetrical structures as shown in Fig. 4 b. In this way, the double deflection can be measured. Under-etching and technology variations

are eliminated. The stress can also be calculated using the Eq. (10). The other improved test structure is the *folded indicator structure* [28]. This design was used to minimize the total area of the test structure occupied on the wafer as shown in Fig. 4 c. The stress can be calculated using the simplified Eq. (11).

$$\sigma = \frac{E}{1-\nu}\frac{d}{2l_a l_i}\delta, \tag{10}$$

where δ is the opposite displacement of the two indicators, d, l_a and l_i are defined in Fig. 4 c.

3.2 Micro Strain Gauge

The schematic of the micro strain gauge proposed by Lin et al. [29] is shown in Fig. 5 a. The gauge consists of three beams, a test beam, a slope beam, and an indicator beam for different purposes. The test beam anchored at one end either shrinks (tensile stress) or elongates (compressive strain) after removing the underlying layer. The change in length of the test beam results in a small rotation of the slope beam. The rotation is magnified with the aid of the long indicator beams, which are equipped with a vernier. The displacement (δ) of the indicator can be measured under an optical microscope, and the residual stress is calculated by,

$$\sigma = \frac{2}{3}\frac{E}{1-\nu}\frac{L_{sb}}{L_{ib}L_{tb}}\delta, \tag{11}$$

where L_{sb}, L_{ib} and L_{tb} are the lengths of the slope beam, indicator beam and test beam, respectively.

3.3 Long-Short Beam Strain Sensor

The long-short beam strain sensor is designed by Pan and Hsu [30], Fig. 5 b schematically shows the strain sensor. The sensor is comprised of a pair of long and short cantilever test beams with different lengths, long test beam

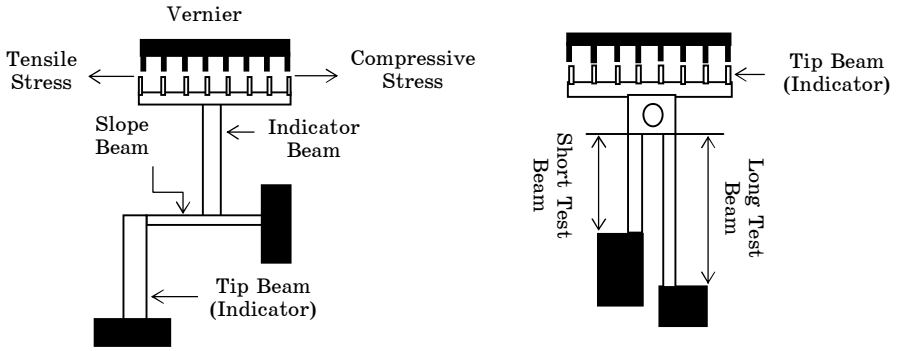

***Fig. 5** – The schematic of micro strain gauge (a) and long-short beam strain sensor (b)*

and short test beam. The two beams are connected by a tip beam as an indicator. After the freestanding part is released, the two test beams will extend or contract due to residual stress in the thin film. The displacement (δ) caused by the deflection of two test beams can be read out using indicator and vernier by optical microscope or SEM. The stress is calculated by,

$$\sigma = \frac{E}{1-\nu}\gamma\delta, \tag{12}$$

where γ is the conversion factor related to geometrical parameters of the structure only.

3.4 Bent-Beams

Bent-beams [31] also take advantage of geometric layout to amplify in-plane displacements induced by residual stress. Bent-beams are capable of measuring compressive and tensile residual stress, indicating compression by a decrease in the distance between the indicators and tension by an increase. Resolution depends on layout geometry. If resolution at low stress values is desired, then L_{BB} must be large. However, this increases the proclivity of the structure to buckle out-of-plane. In this structure optical method allows for rapid and noncontacting measurements. While scanning electron microscopy (SEM) metrology enables higher resolution for in-plane measurements.

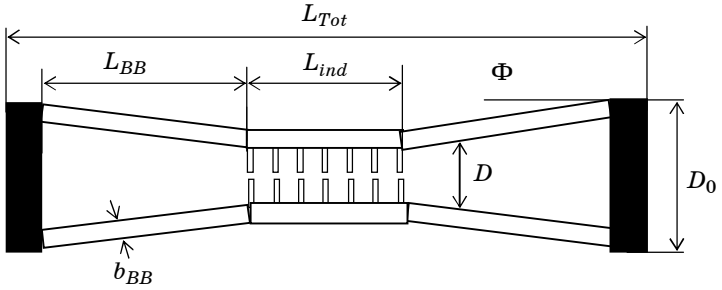

Fig. 6 *– The schematic of bent beam structure*

4. CONCLUSIONS AND SUMMARY

In this paper, we have (i) identified the mechanical properties of interest for the design of microsystems, (ii) cataloged and critically compared the various test techniques (Table 1), and (iii) suggested a rational approach for the selection of test methods for microsystems design.

The details of specimen preparation, experimentation, and data analyses are contained in the cited literature. Several types of stress measurement methods have been reviewed. We have designed mask of test devices for each method. The appendix contains SEM micrographs of fabricated test structures in Fig. A-F. The in situ residual stress measurement will be carried out for plated gold film using these structures. The Table 2 summarizes the theoretical and practical residual stress test structure comparisons.

5. ACKNOLEDGEMENT

Authors would like to acknowledge Director, CEERI, Pilani, for providing the design and fabrication facilities and thankful to all colleagues of Sensors and Nanotechnology Group; who helped in the fabrication of structures.

Table 1 *– Capabilities and characteristics of Test structures compatible with various test techniques*

Test	E	σ_R	σ_y	σ_F	T	F_S	I
Tension	+		+	+	+	+	
Microbeam bend	+		+	+	+	+	
Buldge test	+	+			+	+	
M-test	+	+					+
Wafer curvature		+			+	+	
Strain gauges		+			+	+	+
Stress test method		+			+	+	+

E – Young modulus, σ_R – residual stress, σ_y – yield stress, σ_F – fracture stress, T – thin, F_S – free standing, I – integrated.

Table 2 *– Theoretical and practical residual stress measurement test structure comparisons*

Types	Beams	Cantilevers	Microrings		Pointers	Bent-beams
			Guckel	Diamond		
Principle of structure	Buckling converted into compressive stress	Buckling converted into stress gradient	Conversion of buckling to tension	Conversion of buckling to tension and compression	Geometrical amplification	Geometrical amplification
Resolution (με)	0.7 (± 0.35)	-	50	-	40(O = 20 μm) 99(O = 60 μm) [32]	12.5 (L_{BB} = 300 μm, Φ = 33.3 mrad 5 (L_{BB} = 500 μm, Φ = 20 mrad)
Layout Dimensions of Test Structures in the Class	L_B = 40-140 μm b_B = 10-30 μm Δ = 10 μm	L_{CB} = 50-280 μm b_{CB} = 15-30 μm	L_t = 15μm W_t = 20μm b_r = 14μm b_b = 5μm R = 100-10 μm, Ring I_D = 40-200 μm	L_4 = 10-100 μm L_3 = 10-200 μm b_1 = 20 μm b_2 = 10 μm	L_A, L_B = 490 μm W = 20 μm O = 20 μm (C_F = 0.425), O = 40 μm (C_F = 0.530), O = 60 μm (CF = 0.539), (with L_C = 585, 575, 565 μm, respectively)	b_{BB} = 2 μm D = 38.5 μm L_{Ind} = 98 μm Φ = 33.3, 66.7 and 135.4 mrad (LBB = 300 μm) Φ = 20.0, 20.0** and 79.5 mrad (L_{BB} = 500 μm)
Area	0.1 mm^2	0.1 mm^2	0.8-1 mm^2	1 mm^2	0.8-1.5 mm^2	0.08-0.2 mm^2
Displacement	0.5μm [33]	0.4 μm	0.4 μm [33]	0.3 μm [33]	1-7 μm [34]	3μm [31]

REFERENCES

1. J.M. Bustillo, R.T. Howe, R.S. Muller, *Proc. IEEE* **86**, 1552 (1998).
2. S.D. Senturia, *Proc. Transducers'87*, 11 (Tokyo: Japan: 1987).
3. James J. Allen, *Micro Electro Mechanical System Design,* 96 (Taylor & Francis London: UK: 2005).
4. H.-J. Lee, G.Cornella, J.C. Bravman, *Appl. Phys. Lett.* **76,** 3415 (2000).
5. S. Greek, et al. *MRS Symposium Proceedings*, **518**, 51 (1998).
6. M.A. Haque, M.T.A. Saif, *Exp. Mech.* **42,** 123 (2002).
7. W.N Sharpe, Jr., B. Yuan, R.L. Edwards, *J. Microelectromech. S.* **6**, 193 (1997).
8. J.A. Ruud, D. Josell, F. Spacpcn, A.L. Greer, *J. Mater. Res.* **8**, 112 (1993).
9. H. Huang, F. Spaepen, *Acta Mater.* **48**, 3261 (2000).
10. F. Ericson, J.-A. Schweitz, *J. Appl. Phys.* ***68***, 5840 (1990).
11. S. Johansson, F. Ericson, J-A Schweitz, *J. Appl. Phys.* **65**, 122 (1989).
12. T.P. Weihs, S. Hong, J.C. Bravman, W.D. Nix, *J. Mater. Res.* **3**, 931 (1988).
13. T.Y. Zhang, Y.J. Su, C.F. Qian, M.H. Zhao, L.Q. Chen, *Acta Mater.* **48**, 2843 (2000).
14. T.P. Weihs, S. Hong, J.C. Bravman, W.D. Nix, *J. Mater. Res.* **3**, 931 (1988).
15. D. Maier-Schneider, J. Maibach, E. Obermeier. *J. Microelectromech. S.* **4**, 238 (1995).
16. J.J. Vlassak, W.D. Nix *J. Mater. Res.* **7**, 3242 (1992).
17. O. Tabata, K. Kawahata, S. Sugiyama, I. Igarashi, *Sensor. Actuat.* **20**, 135 (1989).
18. P.M. Osterberg, S.D. Senturia, *J. Microelectromech. S.* **6**, 107 (1997).
19. B.D. Jensen, M.P. de Boer, N.D. Masters, *J. Microelectromech. S.* **10**, 336 (2001).
20. W.D. Nix, *Metal. Trans. A* **20**, 2217 (1989).
21. Y.J. Kim, M.G. Allen, *IEEE Trans. Compon. Pack.* **22,** 282 (1999).
22. S. Suresh, A.E. Giannakopoulos, *Acta Mater.* **46**, 5755 (1998).
23. U. Welzel, J. Ligot, P. Lamparter, A.C. Vermeulen, E.J. Mittemeijer, *J. Appl. Crystallogr.* **38**, 1 (2005).
24. H. Guckel, T. Randazzo, D.W. Burns, *J. Appl. Phys.* **57**, 1671 (1985).
25. H. Guckel, D.W. Burns, C.C.G. Visser, H.A.C. Tilmans, D. Deroo, *IEEE T. Electron Dev.* **35**, 800 (1988).
26. B.P. van Drienhuizen, J.F.L. Goosen, P.J. French, R.F. Wolffenbuttel, *Sensor Actuat. A-Phys.* **37/38**, 756 (1993).
27. J.F.L. Goosen et al., *Proc. Transducers'93*, 783 (Tokyo: Japan: 1993).
28. F. Ericson, S. Greek, J. Soderkvist, J.-A. Schweitz, *J. Micromech. Microeng.* **7**, 30 (1997).
29. L. Liwei, A.P. Pisano, R.T. Howe, *J. Microelectromech. S.* **6**, 313 (1997).
30. C.S. Pan, W. Hsu, *J. Microelectromech. S.* **8**, 200 (1999).
31. Y.B. Gianchandani, K. Najafi, *J. Microelectromech. S.* **5**, 52 (1996).
32. Masters, et al. *American Society for Testing and Materials* 33 (2001).
33. Q. He, Z.X. Luo, X.Y. Chen, *Thin Solid Films* **516**, 5318 (2008).
34. A. Sharma, K. Rangra, M. Kaur, D. Kumar, http://www.comsol.fi/papers/8084.

APPENDIX

The fabricated electroplated gold Test structures SEM micrographs for mechanical parameter extraction.

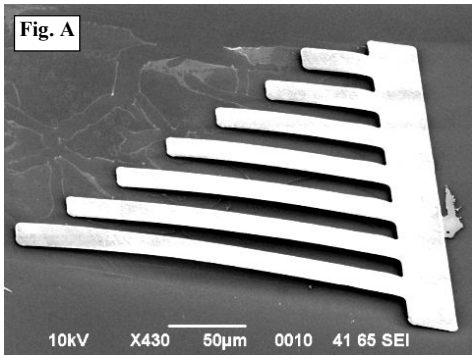

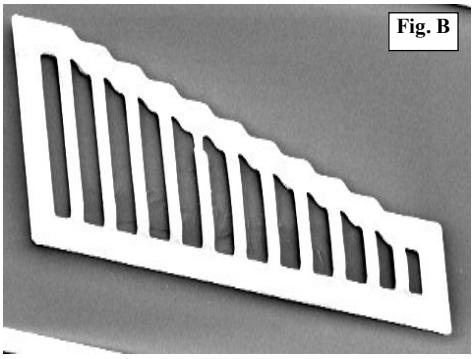

Fig. A – Cantilevers array for stress gradient measurement
Fig. B – Fixed-2 beam array for compressive stress measurement

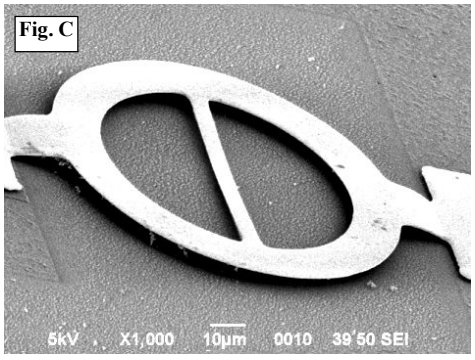

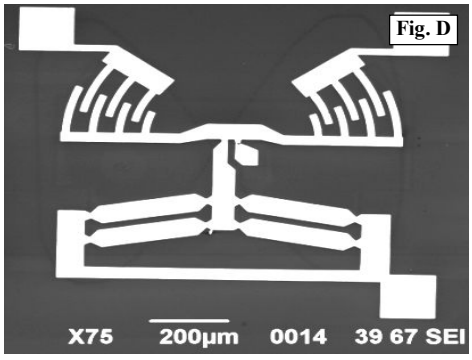

Fig. C – Gьckel Ring for Tensile stress measurement
Fig. D – Modified rotational type test structure

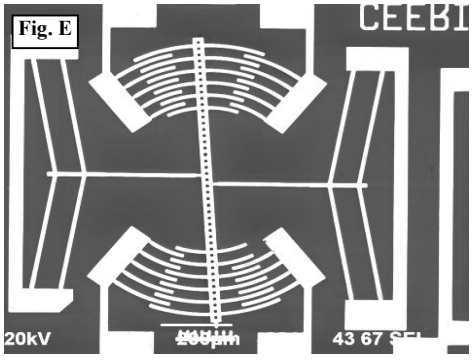

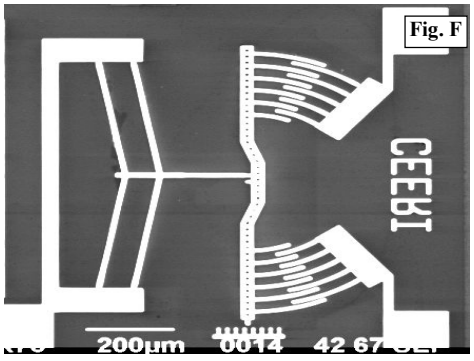

Fig. E – Asymmetrical rotational lancet pointer structure
Fig. F – Symmetrical rotational lancet pointer structure